Simulation and Prediction of the MJO with the NCEP models

Wanqiu Wang, Suranjana Saha*, and Hua-Lu Pan*

SAIC at National Centers for Environmental Prediction, Camp Springs, Maryland
**Environmental Modeling Center, National Centers for Environmental Prediction, Camp Springs, Maryland*

Abstract

This study investigates the impact of the air-sea interaction on the simulation and prediction of the Madden-Julian Oscillation (MJO) by the National Centers for Environmental Prediction atmospheric Global Forecast System model (GFS03) and Coupled atmosphere-ocean Forecast System model (CFS03). Comparison between simulations by GFS03 and CFS03 indicates that the coupling improves the coherence between convection and circulation and the organization of eastward-propagating anomalies. The MJO simulated by CFS03 is greatly strengthened compared with that by GFS03, and is too strong and a little too slow compared with that observed. The forecast experiments with GFS03 and CFS03 suggest that air-sea coupling is necessary for MJO forecast beyond two weeks. Forecast MJO activities after two-week integrations with GFS03 become very week, while CFS03 maintains eastward-propagating strong anomalies throughout forecast integrations of 30 days.

1. Introduction

Since the discovery of the tropical Madden-Julian Oscillation (MJO) three decades ago (Madden and Julian, 1971; Madden and Julian, 1972), most of the studies on the MJO have considered it a result of internal atmospheric dynamics involving the interaction between the convection and large-scale circulation. While some characteristics of the MJO can indeed be simulated by atmospheric models with prescribed sea surface temperatures (e.g., Hayashi and Golder, 1986; Wang and Schlesinger, 1999), a few recent studies suggest that air-sea coupling may be another important process in the MJO dynamics. Flatau *et al*. (1997) and Hendon and Glick (1997) showed observational evidence that there is a significant relationship among the convection, SSTs, latent heat flux, and insolation, with positive SST anomalies to the east of convective heat source due to reduced evaporation and/or increased insolation, and with negative SST anomalies under and to the west of the convective heat source due to enhanced evaporation and/or reduced solar flux. A few modeling studies have indicated that the inclusion of the air-sea interaction improves the simulation of several aspects of the MJO, including the seasonality, coherence between circulation and convection, and propagation (Waliser *et al*., 1999; Iness and Slingo, 2003; Kemball-Cook *et al*., 2003).

One aspect of the studies on the MJO is its predictability and its role in the forecast of the extratropical fluctuations. Ferranti *et al*. (1990) demonstrated that the extended-range weather forecasts by the European Center for Medium-Range Forecasts (ECMWF) model would be significantly improved if the MJO activities in the tropics had been realistically captured by the modal. The prediction of the MJO itself, however, has not been successful. Lau and Chang (1992) showed that forecast of eastward propagation intraseasonal mode by previous versions of the National Centers for Environmental Prediction (NCEP) Medium-Range Forecast model (MRF86 and MRF87) were skillful only for the first 10-day forecast period. Hendon *et al*. (2000) and Jones *et al*. (2000) found that the more recent reanalysis version (Kalnay *et al*., 1996) of the NCEP MRF model was not capable of capturing the observed strong MJO activities in the tropics. It is not clear what are the causes of the failure of the MJO forecast in these studies. One of the possible reasons is that the atmospheric dynamics of the MJO were not well represented in the atmospheric model, as implied in the study of Jones *et al*. (2000) who showed that a ten-year run with the atmospheric model used in their MJO forecast did not reproduce the observed MJO with reasonable amplitude and phase speed. Another reason is

that certain physical processes, for example, the air-sea-interaction, were not included in the forecast models. If SSTs are not import, the forecast would not be sensitive to the treatment of the ocean surface. If the air-sea interaction is an important process, a coupled atmosphere-ocean model would be necessary for a realistic forecast of the MJO.

A new global coupled atmosphere-ocean forecast system model (CFS03) has recently been developed at the National Centers for Environmental Prediction (NCEP). It consists of the latest version of the NCEP atmospheric Global Forecast System model (GFS03) and the Geophysical Fluid Dynamics Laboratory (GFDL) Modular Ocean Model V.3 (MOM3). In this study, we investigate the role of the air-sea interaction on the simulation and prediction of the MJO using CFS03 and GFS03. We will first examine results from two twenty-one-year runs: one by the uncoupled atmospheric model (GFS03) with prescribed SSTs and the other by the coupled atmosphere-ocean model (CFS03). Comparison between these two runs indicates that the coupling improves the coherence between convective heating and large-scale circulation, and enhances the amplitude of the simulated MJO. We will then explore the influence of the inclusion of an interactive ocean on the forecast of the MJO by comparing the performance of 30-day forecast by CFS03 and GFS03 for the boreal cold seasons of 2000/2001 and 2002/2003. We have found that the inclusion of an interactive ocean helps maintain the strength of the eastward propagating anomalies associated with the MJO.

2. The models and observational data

The atmospheric model used in this study is the current version of the NCEP Global Forecast System model (GFS03). It adopts a spectral truncation of 62 waves (T62) in the horizontal (equivalent to nearly a 200-km grid) and a finite differencing in the vertical with 64 sigma layers. The top of the model atmosphere is at 0.2 hPa. GFS03 was modified from the version of the NCEP model used for the NCEP/NCAR Reanalysis (Kalnay *et al*, 1996) with upgrades in the physics of solar radiation (Hou, 1996), boundary layer vertical diffusion (Hong and Pan, 1996), cumulus convection (Hong and Pan, 1998), gravity wave drag (Kim and Arakawa, 1995), and cloud water/ice (Zhao and Carr, 1997).

The coupled model (CFS03) consists of GFS03 and the GFDL Modular Ocean Model V.3 (MOM3) (Pacanowski and Griffies, 1998). MOM3 is a finite difference version of the ocean primitive equations under the assumption of the Boussinesq and hydrostatic approximations. It uses spherical coordinates in the horizontal with a staggered Arakawa B grid and the z-coordinate in the vertical. The ocean surface boundary is computed as an explicit free surface. The domain is quasi-global extending from 74°S to 64°N. The zonal resolution is 1°. The meridional resolution is 1/3° between 10°S and 10°N, gradually increasing through the tropics until becoming fixed at 1° poleward of 30°S and 30°N. There are 40 layers in the vertical with 27 layers in the upper 400 m and the bottom depth is around 4.5 km. The vertical resolution is 10 m from the surface to the 240-m depth, gradually increasing to about 511 m in the bottom layer. Vertical mixing follows the non-local K-profile parameterization of Large *et a*l. (1994). The horizontal mixing of tracers uses the isoneutral method pioneered by Gent and McWilliams (1990) (see also Griffies *et al*., 1998). The horizontal mixing of momentum uses the nonlinear scheme of Smagorinsky (1963).

In CFS03, the atmospheric and oceanic components are coupled without any flux adjustment. The two components exchange daily averaged quantities once a day. Because of the difference in latitudinal domain, full interaction between GFS03 and MOM3 is confined to 65°S to 50°N. Poleward of 74°S and 64°N, the SSTs are taken from observed climatology. Between 74°S and 65°S, and between 64°N and 50°N, SSTs are weighted average of the observed climatology and MOM3 with the weight linearly varying with latitude, such that the SSTs at 74°S and 64°N equal observed climatology and at 65°S to 50°N the SST's equal values from MOM3. Sea ice extent is prescribed from the observed climatology. CFS03 has been found to reproduce a realistic climatology of SSTs in the tropics with the amplitude of mean errors being generally less than 1 K.

For evaluation of the performance of CFS03 and GFS03, simulations and forecast by the models will be compared with the NCEP/DOE Reanalysis-2 (R2) (Kanamitsu *et al*., 2002) and the Climate Prediction Center merged analysis of precipitation (CMAP) (Xie and Arkin, 1997).

3. The MJO simulated by GFS03 and CFS03

In this section we present the impact of the inclusion of the air-sea interaction on the simulated MJO by comparing two runs: one run is a 21-year simulation with GFS03 using prescribed monthly mean SSTs of 1982-2002 and the other is a 21-year free run with CFS03. For comparison with the models, R2 and CMAP for 1982-2002 will be used. We will first look at the wavenumber-frequency power spectra of tropical 850 hPa zonal velocity. We will then examine the leading combined patterns of the tropical intraseasonal variability of precipitation, 850 hPa zonal velocity, and 200 hPa zonal velocity, and the temporal evolution of the associated fields.

3.1. Power spectra of tropical 850 hPa zonal velocity

Fig. 1 shows wavenumber-frequency power spectra of 10°S-10°N mean 850 hPa zonal velocity (u850). Seasonal cycle defined as the sum of the annual-mean and first 3 harmonics of the long-term daily climatology has been removed before the calculation of the spectra. The spectra from R2 (Fig. 1a) are characterized by an eastward-propagating wavenumber-1 peak around the period of 50 days. GFS03 simulated large eastward-propagating wavenumber-1 variance throughout the intraseasonal period range of

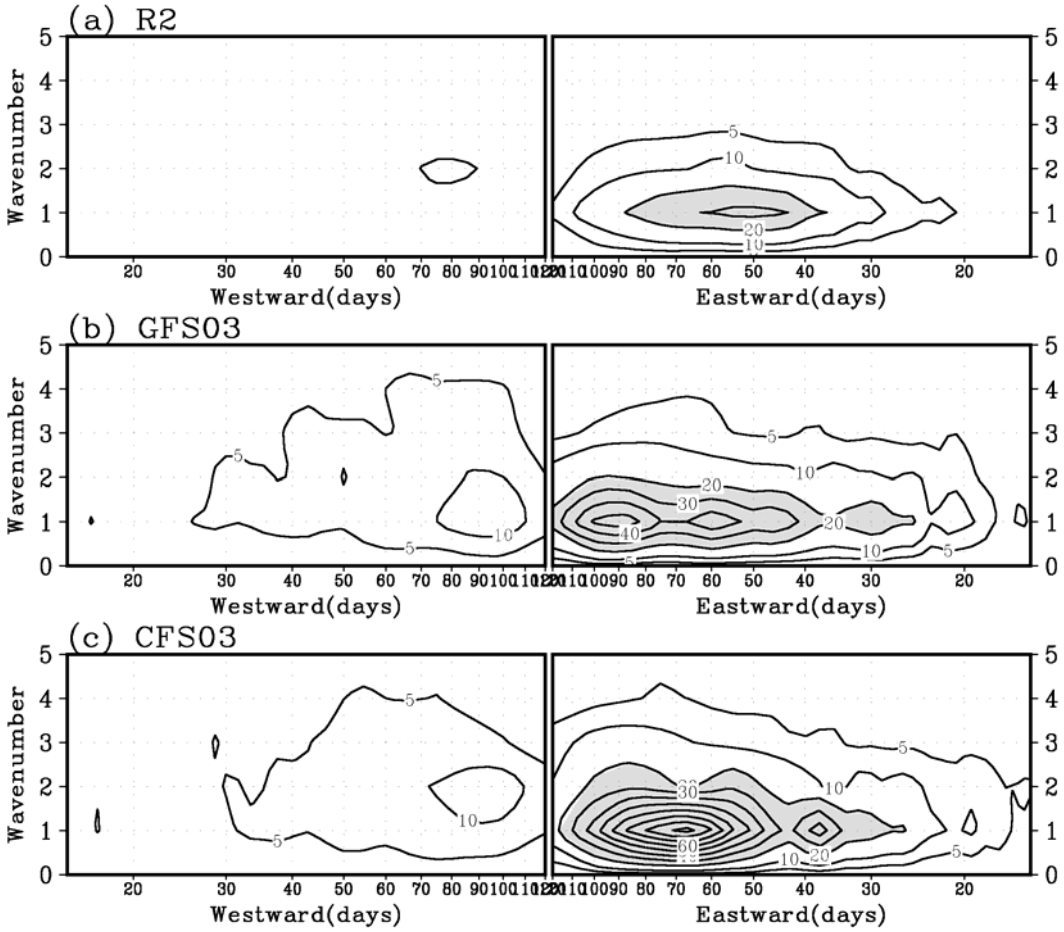

Figure 1: Wavenumber-frequency spectra of 10S-10N mean 850hPa zonal velocity (m2s-2day) from (a) R2, (b) GFS03, and (c) CFS03. Contours are plotted at 5, 10, 20, 30, 40, 50, 60, and 70. Values greater than 20 are shaded.

20-100 days with a peak near 60-day period and another peak near 90-day period (Fig. 1b). Compared with GFS03, the variance in coupled run with CFS03 (Fig 1c) is substantially enhanced with a strong peak near 66-day period. The amplitude of the spectra from CFS03 simulation is about twice as large as that from R2, indicating that the intraseasonal anomalies in CFS03 simulation are about 40 percent stronger than that in R2.

3.2. EOF modes of combined fields

Emperical Orthogonal Functions (EOFs) of combined fields of 10-100-day filtered 10°S-10°N average of 850 hPa zonal velocity (u850), 200 hPa zonal velocity (u200), and precipitation are calculated to identify the MJO. The EOF calculation has been done only for November 1 to March 31 to focus on the eastward propagating modes. For the analyses, u850 and u200 were taken from R2 and precipitation was taken from CMAP. In EOF1 from R2/CMAP (Fig. 2a), strong convective heating source and sink are seen in the Indian Ocean (60°E to 90°E) and in western Pacific near the date line. The convective heat source in the Indian Ocean approximately corresponds to convergent flow in the lower troposphere and divergent flow in the upper troposphere. EOF2 from R2/CMAP (Fig. 2b) is dominated by a strong convective heat source in the maritime continents and western Pacific (90°E-180°E), and the consistent convergent flow in the lower troposphere and divergent flow in the upper troposphere.

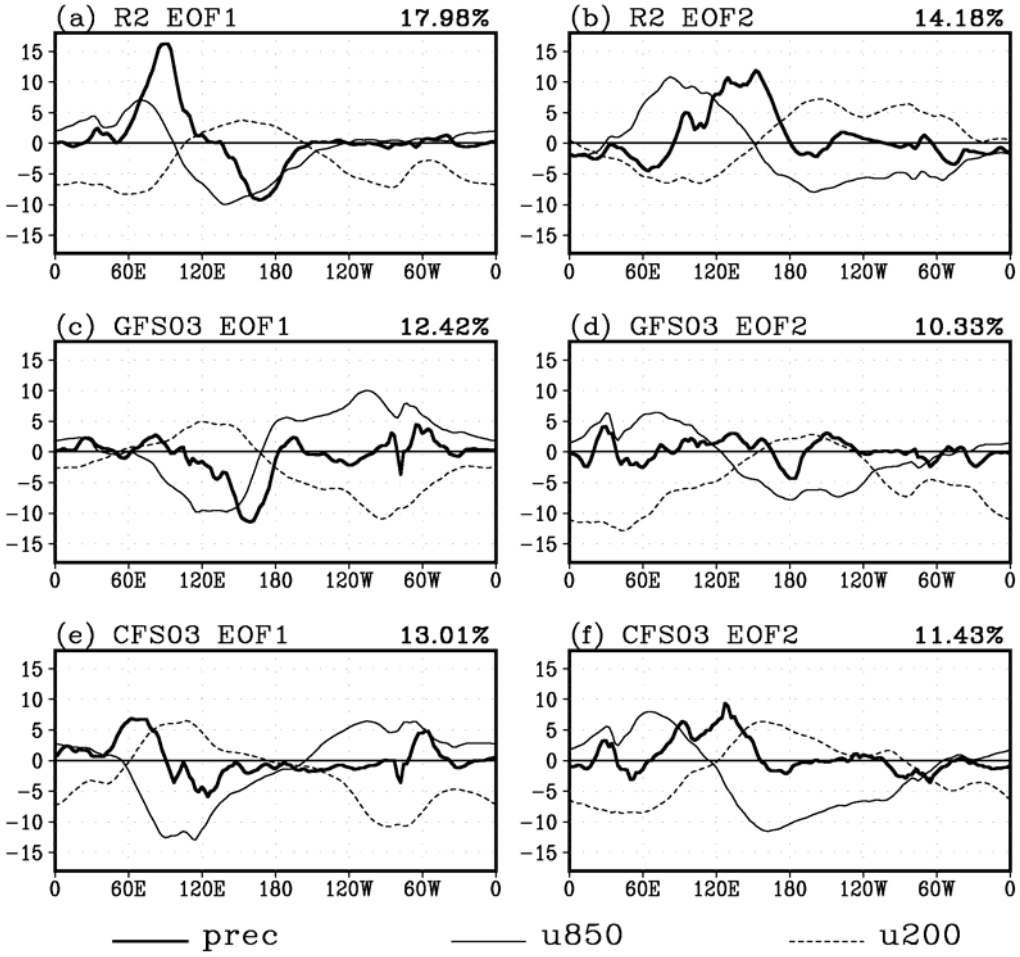

Figure 2: Patterns of Combined empirical orthogonal functions (EOFs) of 10-100 day filtered precipitation, 850hPa zonal velocity (u850), and 200hPa zonal velocity (u200). (a) EOF1 from R2, (b) EOF2 from R2, (c) EOF1 from GFS03, (d) EOF2 from GFS03, (e) EOF1 from CFS03, and (f) EOF2 from CFS03. Thick solid curves are precipitation, thin solid curves are u850, and thin dashed curved are u200. The percentage value above each panel is the variance explained by each mode.

GFS03 reproduced the observed heating source in the Indian-Ocean in EOF1 and the heating source over maritime continents and western Pacific in EOF2, but with much weaker amplitude (Figs. 2c and 2d). The Indian-Ocean convective heating source in EOF1 in CFS03 run (Fig. 2e) was stronger than that in GFS03 run, but was located to the west of the observed. CFS03 simulated a realistic heating source over the maritime continents and western Pacific (90°E-180°E) in EOF2 (Fig. 2f). Overall, the coupling of the atmospheric component (GFS03) to MOM3 in CFS03 improves the coherence between the convective activities and large-scale circulation.

3.3. Propagation and relationship among associated fields

To examine the propagation and the relationship among different fields, we calculated lag correlation between principal component of EOF1 (PC1) and individual fields. The lag correlation between principal component of EOF2 (PC2) and individual fields reveals similar features except that the entire patterns are shifted eastward, and will not be shown.

A consistent eastward propagation is seen in u850 and precipitation from the analyses (Figs. 3a and 3d). The analysis also shows that surface shortwave radiation flux anomalies (SW) are positive to the east of positive precipitation anomalies (Fig. 3g). Latent heat flux (LH) (Fig. 3j) is also found to propagate eastward with largest amplitude located in the western Pacific (110°E-170°E). The evolution of SST (Fig. 3m) also appears to propagate eastward coherently. These features are qualitatively consistent with the conceptual model proposed by Flatau et al. (1997).

Both GFS03 and CFS03 simulated the eastward propagating feature in u850, precipitation and SW, but the coherence between the circulation field (u850), precipitation and SW, and the organization of the eastward propagation appear to be improved in CFS03 compared with those in GFS03 (Figs. 3b, 3c, 3e, 3f, 3h, and 3i). The eastward propagation of LH in the simulation by CFS03 (Fig. 3l) does not appear to be as realistic as that by GFS03 (Fig. 3k). While GFS03 captured the large amplitude in LH over the western Pacific (Fig. 3k), CFS03 did not reproduce a correlation of any appreciable amplitude between 130°E and 180°E (Fig. 3l) as found in R2 (Fig. 3j). As discussed in Inness and Slingo (2003), the mean surface wind is important in determining the LH anomalies. If the mean surface wind is the major factor controlling the distribution of LH, the positive LH correlation (between 130°E and 180°E) to the east of the convection in R2 and GFS03 (Figs. 3j and 3k) should correspond to mean westerlies in the western Pacific. The inconsistent LH in CFS03 with that in R2 may be due to errors in the time mean of surface wind. To explore this possibility, we calculated the climatology of 1000 hPa zonal velocity. As shown in Fig. 4, mean westerlies are found in the western Pacific between the equator and 10°S in both R2 and GFS03 (Figs. 4a and 4b), while CFS03 simulated weak easterlies in this area. This suggests that the weak correlation near zero time-lag in the western Pacific in CFS03 simulation (Fig. 3l) is related to the errors in mean surface wind.

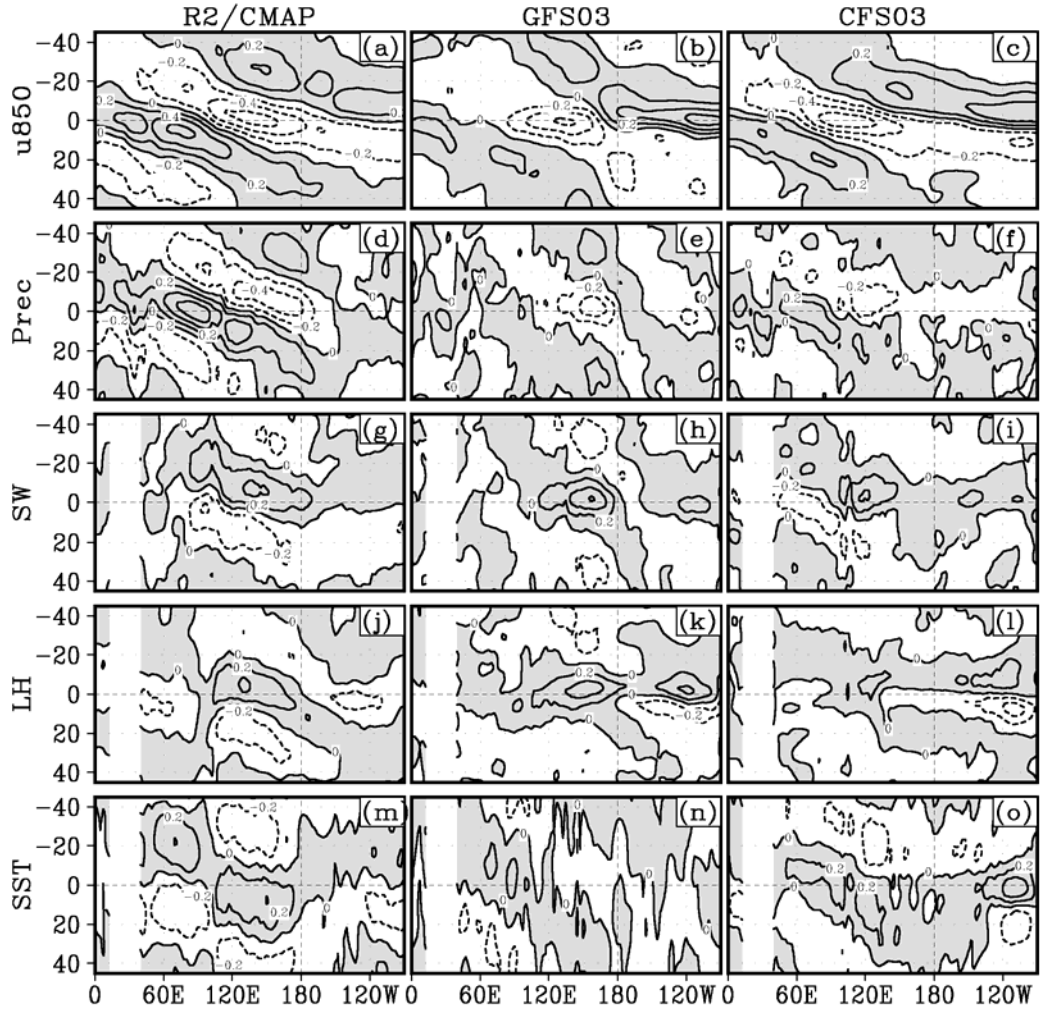

Figure 3: Lag correlation between EOF1 principal component (PC1) and (a) 850 hPa zonal velocity (u850) from R2, (b) u850 from GFS03, (c) u850 from CFS03, (d) precipitation from CMAP, (e) precipitation from GFS03, (f) precipitation from CFS03, (g) surface net down ward solar radiation (SW) from R2, (h) SW from GFS03, (i) SW from CFS03, (j) surface downward latent heat flux (LH) from R2, (k) LH from GFS03, (l) LH from CFS03, (m) SST used in R2, (n) SST used in GFS03, and (o) SST from CFS03. SW, LH, and SST are plotted only for ocean surface. Positive values are shaded.

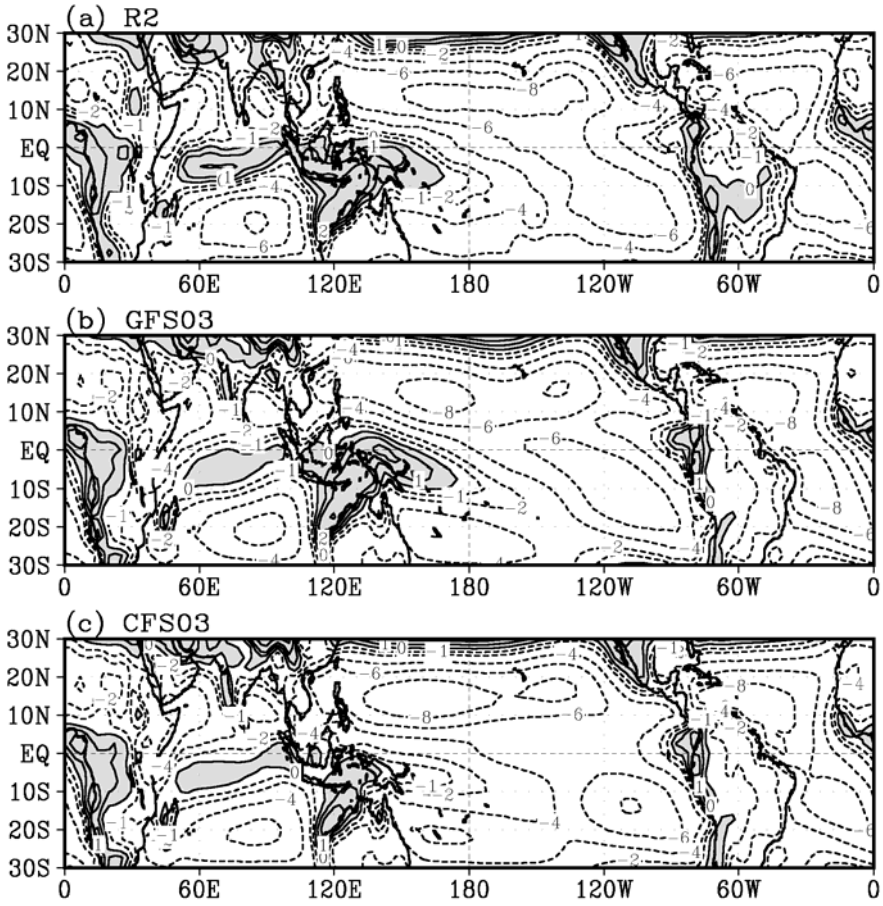

Figure 4: November-March time-mean 1000hPa zonal velocity (m/s). (a) R2, (b) GFS03, and (c) CFS03. Contours are plotted at –8, -6, -4, -2, -1, 0, 1, 2, 4, 6, and 8. Positive values are shaded.

CFS03 simulated the eastward propagating feature in SST as in the observation (Figs. 3m and 3o), although some differences in details exist between CFS03 and R2. One surprising feature in Fig 3 is that even the SST field in GFS03 simulation shows an eastward propagation feature (Fig. 3n), indicating that at least part of the intraseasonal variability associated with EOF1 is model's response to the prescribed SST anomalies. A 21-year run was made with GFS03 using climatological SSTs to further test this. Wavenumber-frequency spectra of u850 from this run are shown in Fig. 5. It is noticed that the peak near 90-day period in GFS03 run with observed monthly-mean SSTs (Fig. 1b) does not appear in Fig.5. The lag correlation between PC1 and u850, precipitation, SW, and LH shows similar features to those in the GFS03 simulation with observed monthly SSTs but with faster eastward propagation (not shown). This demonstrates that the intraseasonal variability in the simulation with GFS03 with observed monthly-mean SSTs indeed contains response to SST anomalies.

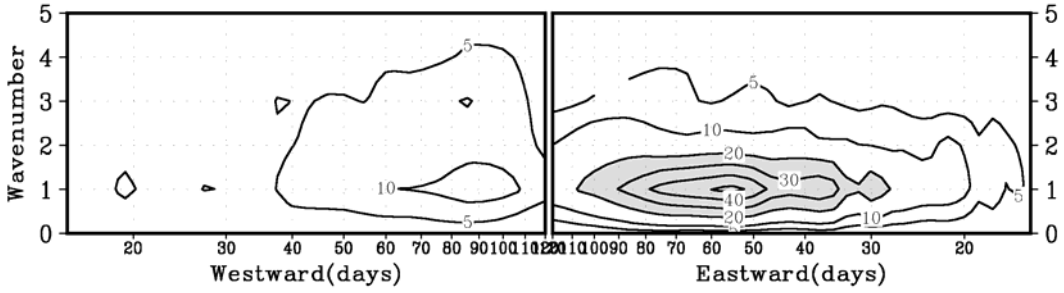

Figure 5: As in Fig. 1, except for an uncoupled run with GFS03 using climatological SSTs.

4. Forecast experiments of the MJO by GFS03 and CFS03

While the comparison in the MJO simulation between the uncoupled atmospheric model and the coupled atmosphere-ocean model may help understand the role of are-sea coupling, it is also interesting and desirable to examine the necessity of the use of an interactive ocean in the forecast of the MJO. In this section we compare the results from forecast experiments using GFS03 with that using CFS03. Forecast has been made once per day for initial conditions of the 120-day cold season of November 1 to February 28 for 2000/2001, 2001/2002, and 2002/2003. In this preliminary study, we will only diagnose the forecast for strong eastward-propagating MJO events. The events are selected based on the amplitude of principal components (PC1 and PC2) of the two leading modes of the combined EOFs of 10°S-10°N mean u850, u200, and precipitation, and based on the coherence of PC1 and PC2. An event is selected if its amplitude of PC1 and PC2 is greater than 1 standard deviation and if the lag between PC2 peak and PC1 peak is between 8 and 17 days. Four events are found to satisfy these criteria: two are in the cold season of 2000/2001, and the other two in the cold season of 2002/2003. The time series of PC1 and PC2 are shown in Fig. 6 and the dates of PC1 and PC2 peak values are listed in Table 1.

PC1 peak	**PC2 peak**
19 November 2000	29 November 20000
25 January 2001	10 February 2001
12 November 2002	23 November 2002
24 December 2002	1 January 2003

Table 1 Dates of peak values of PC1 and PC2 in the seasons of November 1 to February 28 of 2000/2001, and 2002/2003

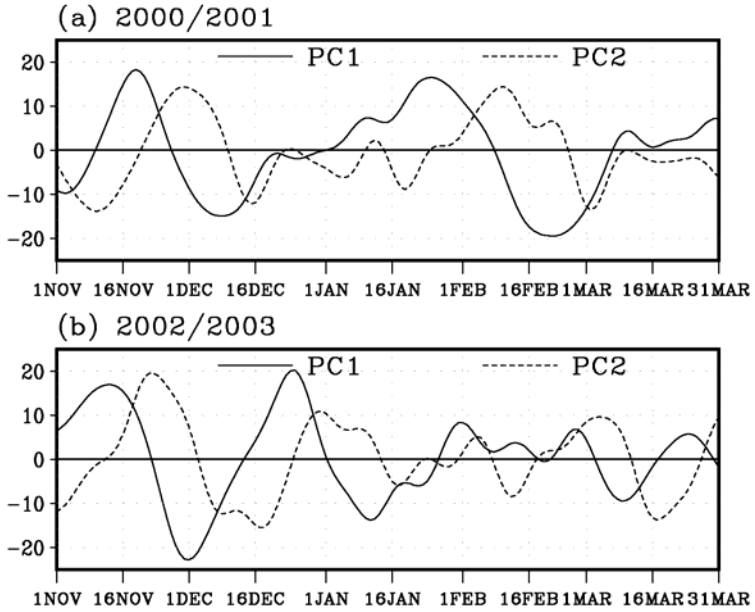

Figure 6: Principal components of EOF1 (PC1, solid curves) and EOF2 (PC2, dashed curves) for November 1 to March 31 of (a) 2000/2001 and (b) 2002/2003.

Four forecast experiments have been made (Table 2) to examine the impact of the treatment of the ocean surface. The first experiment (DAMP) was made with GFS03 using damped initial SST anomalies with an e-folding time scale of 90 days. The second experiment (CLIM) was conducted with climatological SSTs. The third experiment (AMIP) was carried out with GFS03 using weekly optimum interpolation (OI) SSTs

analysis of Reynolds *et al*. (2002). The fourth experiment (COUP) was performed with CFS03 using realistic oceanic initial condition from the NCEP global oceanic data assimilation system (Behringer, personal communication).

Experiment	**Description**
DAMP	GFS03 using damped initial SST anomalies
CLIM	GFS03 with climatological SSTs
AMIP	GFS03 with observed weeklt SSTs
COUP	CFS03 with realistic initial oceanic condiction

Table 2: Forecast experiments

The forecast will be presented for four initial phases. Phase 2 initial dates correspond to the peaks of PC1 as shown in Table 1, representing the mature state of the MJO when strong convection is in the Indian. Phases 3 initial dates correspond to the peaks of PC2 in Table 1, representing the mature state of the MJO when strong convection is over the maritime continents and western Pacific. Phase 1 is ten days prior to phase 2, representing the initial stage of MJO events in the Indian Ocean. Phase 4 is ten days after phase 3, representing the weakening stage when the convective heat source propagates eastward out of the western Pacific.

Intraseasonal anomalies are defined as the deviation from a parabolic fit to the 120-day time series for each lead time from 1 day to 30 days for each cold season. The forecast anomalies have been smoothed by averaging the forecast from three adjacent initial dates centered at the specified initial dates of each phase. Composite forecast of u850 anomalies starting from the four initial phases is presented in Fig. 7. Forecast with damped SSTs (DAMP) and forecast with climatological SSTs (CLIM) maintained strong propagating anomalies only for about two weeks (Figs. 7e, 7f, 7g, 7h, 7i, 7j, 7k, and 7l). Forecast with observed SSTs (AMIP) sustained the eastward propagating strong anomalies for most of the 30-day forecast periods (Figs. 7m, 7n, 7o, and 7p), except that the propagating anomalies from phase 2 initial conditions became too weak after 20 days (Fig. 7n). Forecast using an interactive ocean (COUP) maintained strong eastward-propagating anomalies for the entire 30-day forecast period and for all initial phases (Figs. 7q, 7r, 7s, and 7t), suggesting that a coupled model is probably necessary for a satisfactory forecast of MJO activities. Anomalies in the COUP forecast from phase 2 initial conditions, however, seem to propagate too slowly (Fig. 7r).

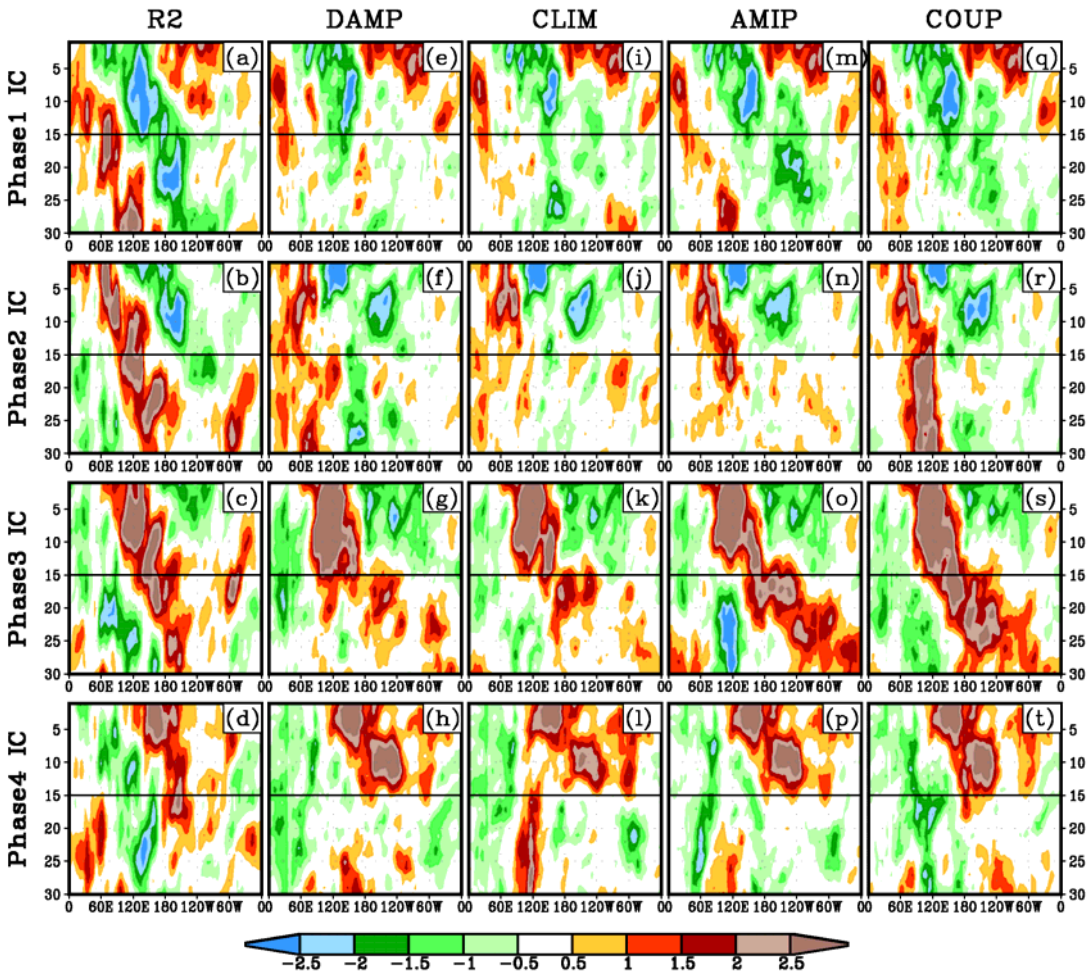

Figure 7: Composite 850 hPa zonal velocity (m/s). (a) R2 from phase 1 initial conditions (ICs), (b) R2 from phase 2 ICs, (c) R2 from phase 3 ICs, (d) R2 from phase 4 ICs, (e) DAMP forecast from phase 1 ICs, (f) DAMP forecast from phase 2 ICs, (g) DAMP forecast from phase 3 ICs, (h) DAMP forecast from phase 4 ICs, (i) CLIM forecast from phase 1 ICs, (j) CLIM forecast from phase 2 ICs, (k) CLIM forecast from phase 3 ICs, (l) CLIM forecast from phase 4 ICs, (m) AMIP forecast from phase 1 ICs, (n) AMIP forecast from phase 2 ICs, (o) AMIP forecast from phase 3 ICs, (p) AMIP forecast from phase 4 ICs, (q) COUP forecast from phase 1 ICs, (r) COUP forecast from phase 2 ICs, (s) COUP forecast from phase 3 ICs, and (t) COUP forecast from phase 4 ICs. Values are shaded at –2.5, -2, -1.5, -1, -0.5, 0.5, 1, 1.5, 2, and 2.5.

SST anomalies in the forecast experiments are shown in Fig. 8. There are some small differences between R2 (Figs. 8a, 8b, 8c, and 8d) and AMIP forecast (Figs. 8m, 8n, 8o, and 8p). This is because R2 and AMIP forecast use different sets of weekly OI SST analysis by Reynolds *et al*. (2002). R2 uses the real-time analysis that was produced daily using available data for the previous seven days. The AMIP forecast experiments use daily SSTs linearly interpolated from the OI analysis produced once per week. Although some details in the COUP forecast appear to be erroneous, the COUP forecast captured some features in the observation. For examples, the COUP forecast reproduced the observed positive anomalies in the western Indian Ocean and negative anomalies in the western Pacific in the second half of the forecast period from phase 1 initial conditions (Figs. 8a and 8q). The observed cold anomalies in the Indian Ocean during the forecast period from phase 2 initial conditions were captured in the COUP forecast (Figs. 8b and 8r). The forecast positive SST anomalies after day 16 in the Indian Ocean in the forecast from phase 3 initial conditions appear to be real (Fig. 8s). The negative SST anomalies in the western Pacific after day 10 in the forecast from phase 3 initial conditions are consistent with the observed but are possibly too strong (Fig. 8s).

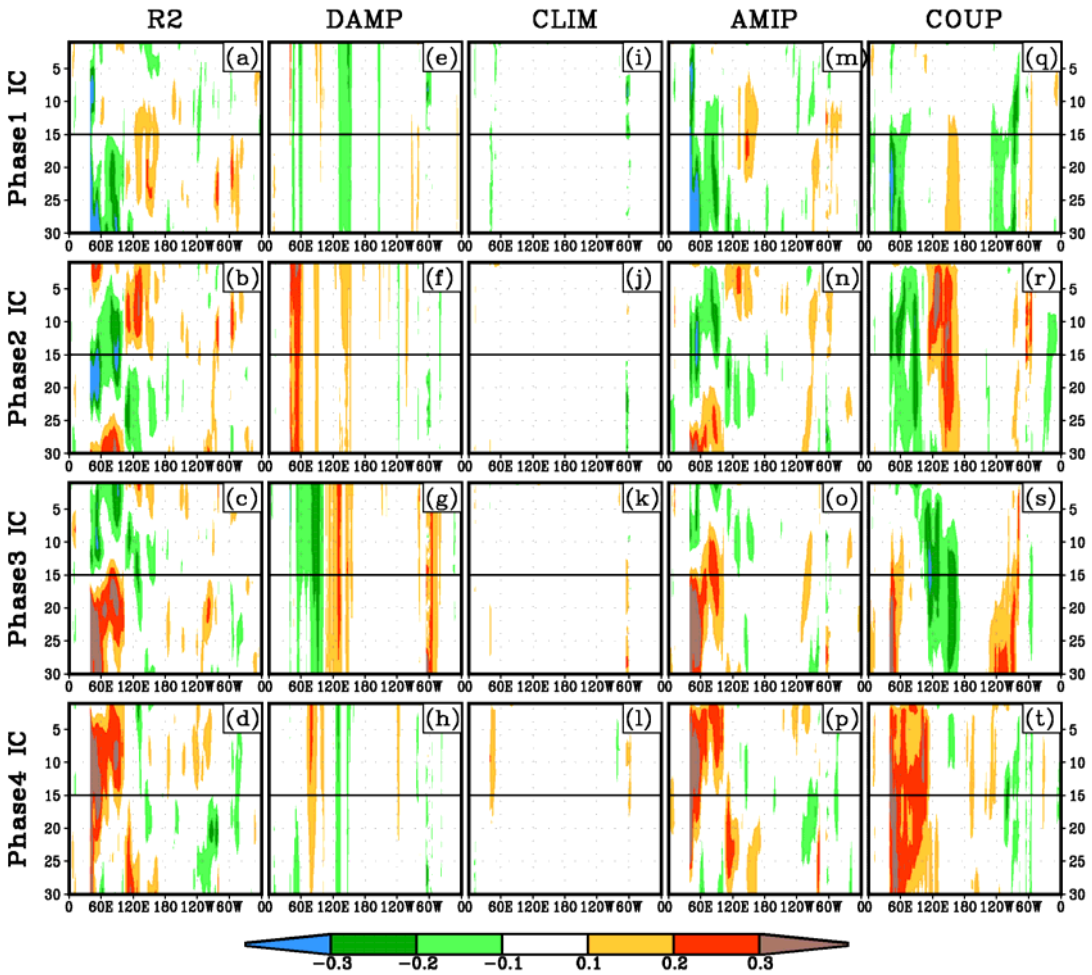

Figure 8: As in Figure 7, except for SST (K). Values are shaded at –0.3, -0.2, -0.1, 0.1, 0.2, and 0.3.

5. Summary

This study investigates the impact of air-sea interaction on the simulation and prediction of the Madden-Julian Oscillation (MJO) by the NCEP atmospheric Global Forecast System model (GFS03) and Coupled Forecast System model (CFS03). Comparison between simulations by GFS03 and CFS03 indicates that the coupling improves the coherence between convection and circulation and the organization of eastward-propagating anomalies. The MJO simulated by CFS03 is greatly strengthened compared with that by GFS03, and is too strong and a little too slow compared with the observation. It is not clear why the MJO simulated by CFS03 is too strong and propagates too slowly. One possible reason is the coupling fashion between the atmosphere and the ocean adopted in the model. In the current CFS03, atmospheric and oceanic components are run sequentially with forcing fields being passed from one component to the other after one-day integration of each component. In the atmospheric component used in this study, SSTs are updated at the end of its one-day integration with daily-mean values passed from the oceanic component. This introduces a delay of the effect of SSTs on the atmospheric fields and may help enhance and slow down the MJO, according to the study by Woolnough *et al*. (2001) who showed that the magnitude of the atmospheric fields increases with decreasing propagating speed of the SST anomalies.

The results from CFS03 simulation are consistent with the conceptual model proposed by Flatau *et al*. (1997) except that latent heat flux pattern in CFS03 is not consistent with that in reanalysis, possibly due to that CFS03 failed to simulate the mean surface westerly in the western Pacific. The simulation by GFS03 indicates that the simulated intraseasonal variability with monthly-mean observed SSTs contains response to

SST anomalies. To completely exclude direct response to SST anomalies in the intraseasonal time range in an uncoupled atmospheric simulation, temporally smoother SSTs should be used.

The forecast experiments with GFS03 and CFS03 suggest that air-sea coupling is necessary for MJO forecast beyond two weeks. Forecast MJO activities after two-week integration with the GFS03 become very week, while CFS03 maintains eastward-propagating strong anomalies throughout integrations of 30 days. The results of MJO forecast in this study, however, are based only on four events and appear to be noisy. Forecast experiments for longer periods are necessary for more statistically significant results.

Acknowledgements

The authors would like to acknowledge the team effort of the NCEP/EMC Global Climate and Weather Modeling Branch, especially J. Alpert, D. Behringer, K. Campana, S. Harper, Y. Hou, M. Iredell, S. Moorthi, J. Sela and D. Stokes.

References

Farranti, L., T. N. Palmer, F. Molteni, and E. Klinker, 1990: Tropical-extratropical interaction associated with the 30-60 day oscillation and its impact on medium and extended range prediction. *J. Atmos. Sci*., **47**, 2177-2199.

Flatau, M., P. J. Flatau, P. Phoebus, and P. P. Niiler, 1997: The feedback between equatorial convection and local radiative and evaporative process: The implication for intraseasonal oscillations. *J. Atmos. Sci*., **54**, 2373-2386.

Gent, P. R. and J. C. McWilliams, 1996: Isopycnal mixing in ocean circulation models. *J. of Phys. Oceanogr*., **26**, 2539-2546.

Griffies, S. M., A. Gnanadesikan, R. C. Pacanaowski, V. Larichev, J. K. Dukowicz, and R. D. Smith, 1998: Isoneutral diffusion in a z-coordinate ocean model. *J. of Phys. Oceanogr*., **28**, 805-830.

Hayashi, Y., and D. G. Golder, 1986: Tropical intraseasonal oscillations appearing in a GFDL general circulation model and FGGE data. Part I: Phase propagation. *J. Atmos. Sci*., **43**, 3058-3067.

Hendon, H. H., and J. Glick, 1997: Intraseasonal air-sea interaction in the tropical Indian and Pacific Oceans. *J. Climate*, **10**, 647-661.

Hendon, H. H., B. Liebmann, M. Newman, and J. D. Glick, 2000: Medium-range forecast errors associated with active episodes of the Madden-Julian Oscillation. *Mon. Wea. Rev*., **128**, 69-86.

Hong, S.-Y. and H.-L. Pan, 1996: Nonlocal boundary layer vertical diffusion in a medium-range forecast model. *Mon. Wea. Rev*., **124**, 2322-2339.

Hong, Song-You, Pan, Hua-Lu. 1998: Convective Trigger Function for a Mass-Flux Cumulus Parameterization Scheme. *Mon. Wea. Rev*., **126**, 2599–2620.

Hou, Y-T, K. A. Campana and S-K Yang, 1996: Shortwave radiation calculations in the NCEP's global model. International Radiation Symposium, IRS-96, August 19-24, Fairbanks, AL.

Inness, P. M., and J. M. Slingo, 2003: Simulation of the Madden-Julian oscillation in a coupled general circulation model. Part I: Comparison with observation and an atmospheric-only GCM. *J. Climate*, **16**, 345-364.

Jones, C., D. E. Waliser, J.K. E. Schemm, and W. K. M. Lau, 2000: Prediction skill of the Madden and Julian Oscillation in dynamical extended range forecasts. *Climate Dyn*., **16**, 273-284.

Kalnay, E., and Coauthors, 1996: The NCEP/NCAR 40-year reanalysis Project. *Bull. Amer. Meteor. Soc*., **77**, 1057-1072.

Kanamitsu, M. , W. Ebisuzaki, J. Woollen, S-K Yang, J.J. Hnilo, M. Fiorino, and G. L. Potter, 2002: NCEP-DEO AMIP-II Reanalysis (R-2). *Bul. of the Atmos. Met. Soc*., 1631-1643.

Kemball-Cook, S., B. Wang, and X. Fu, 2002: Simulation of the intraseasonal oscillation in the ECHAM-4 model: Impact of coupling with an ocean model. *J. Atmos. Sci*., **59**, 1433-1453.

Kim, Y-J and A. Arakawa, 1995: Improvement of orographic gravity wave parameterization using a mesoscale gravity wave model. *J. Atmos. Sci*. 52, **11**, 1875-1902.

Large, W. G., J. C. McWilliams, and S. C. Doney, 1994: Oceanic vertical mixing: A review and a model with nonlocal boundary layer parameterization. *Rev. of Geophys*., **32**, 363-403.

Lau, K.-M., and F. C. Chang, 1992: Tropical intraseasonal oscillation and its prediction by the NMC operational model. *J. Climate*, **5**, 1365-1378.

Madden, R. A., and P. R. Julian, 1971: Detection of a 40-50 day oscillation in the zonal wind in the tropical Pacific. *J. Atmos. Sci*., **28**, 702-708.

Madden, R. A., and P. R. Julian, 1972: Description of global-scale circulation cells in the tropics with a 40-50 day period. *J. Atmos. Sci*., **29**, 1109-1123.

Pacanowski, R. C., and S. M. Griffies, 1998: MOM 3.0 Manual, NOAA/Geophysical Fluid Dynamics Laboratory, Princeton, USA 08542.

Reynolds, R. W., N. A. Rayner, T. M. Smith, D. C. Stokes, and W. Wang, 2002: An improved in situ and satellite SST analysis for climate. *J. Climate*, **15**, 1609-1625.

Smagorinsky, J. 1963: General circulation experiments with the primitive equations: I. The basic experiment. *Mon. Wea. Rev*., **91**, 99-164.

Wliser, D. E., K. E. Lau, and J. H. Kim, 1999: The influence of coupled sea surface temperatures on the Madden-Julian Oscillation: A model perturbation experiment. *J. Atmos. Sci*., **56**, 333-358.

Wang, W., and M. E. Schlesinger, 1999: The dependence on convection parameterization of the tropical intraseasonal oscillation simulated by the UIUC 11-layer atmospheric GCM. *J. Climate*, **12**, 1423-1457.

Woolnough, S. J., J. M. Slingo, and B. J. Hoskins, 2001: The organization of tropical convection by intraseasonal sea surface temperature anomalies. *Quart. J. Roy. Meteor. Soc*., **127**, 887-907.

Xie, P. and P. A. Arkin, 1997: Global precipitation: A 17-year monthly analysis based on gauge observations, satellite estimates and numerical model outputs. *Bull. Amer. Met. Soc*., **78**, 2539-2558.

Zhao, Q. Y., and F. H. Carr, 1997: A prognostic cloud scheme for operational NWP models. *Mon. Wea. Rev*., **125**,1931-1953.